



Short Communication

Pt electrocatalyst-loaded carbon nanofibre–Ru core–shell supports for improved methanol electrooxidation



Geon-Hyoung An, Hyo-Jin Ahn*

Department of Materials Science and Engineering, Seoul National University of Science and Technology, 139-743 Seoul, Republic of Korea

ARTICLE INFO

Article history:

Received 2 June 2013

Received in revised form 23 July 2013

Accepted 20 August 2013

Available online 31 August 2013

Keywords:

Methanol electrooxidation

Carbon nanofibre–ruthenium core–shell supports

Platinum electrocatalyst

Electrospinning

A reduction method.

ABSTRACT

We synthesize Pt electrocatalyst-loaded carbon nanofibre (CNF)–Ru core–shell supports using electrospinning and a reduction method. To investigate the properties of the CNF–Ru core–shell supports, four different loadings of the Ru shell layer are used: 0 wt.% (Pt/CNFs), 10 wt.% (sample A), 20 wt.% (sample B), and 30 wt.% (sample C). Sample B exhibits superior electrocatalytic activity and high electrocatalytic stability as compared to commercial Pt/XC-72, Pt/CNFs, sample A, and sample C. This enhancement could be because of the excellent dispersion of the Pt electrocatalysts, due to the optimum loading of the Ru shell layer on the CNF supports.

© 2013 Elsevier B.V. All rights reserved.

1. Introduction

Direct methanol fuel cells (DMFCs) have recently received considerable attention for their use in powering portable electronic devices because of several advantages such as the high energy density and ease of storage of methanol, low operating temperatures, and formation of environmentally benign products [1–2]. However, the major disadvantages of DMFCs are the high cost and low utilization of the noble Pt electrocatalysts, low electrocatalytic activity at the anode, and methanol crossover [3]. In particular, the need for noble-metal electrocatalysts is the main barrier/bottleneck to the industrial use of DMFCs. Thus, one strategy to solve these problems in DMFCs is to employ effective catalyst supports. The supports reported till date are classified into three categories: carbon-based materials (i.e., carbon black, carbon nanotubes, graphene, and carbon nanofibres (CNFs)), metal oxide-based materials (TiO₂, SnO₂, Sn-doped In₂O₃ (ITO), SiO₂, and WO_x), and conducting polymers (PEDOT, PDDA, and poly(*N*-acteylaniline)) [4]. Among these, carbon-based materials have been intensively studied as supports for electrocatalysts because of their peculiar physical/chemical properties and excellent electrical conductivity as well as their low costs and large surface areas [5–7]. In particular, CNFs have received burgeoning interests as catalytic supports owing to their high aspect ratio, large external surface, small micropores, and stable chemical properties [8]. Many researchers have

devoted their attention to developing CNF supports for DMFCs. For example, Singh et al. fabricated Pt/CNFs for methanol electrooxidation, which showed retention of superior catalytic activity [9]. Kang et al. synthesized PtRu/CNF electrocatalysts for comparison with commercial electrocatalysts and demonstrated their superior electrocatalytic activities [10]. However, the relationship between electrocatalytic activities and the optimum conditions for using Ru shell layers loaded on CNFs as supports in DMFCs has not been studied hitherto. Thus, we have studied Pt electrocatalysts-loaded CNF–Ru core–shell supports that allowed for enhanced methanol electrooxidation for use in DMFCs.

2. Experimental

In order to synthesize the CNFs, a precursor solution of polyacrylonitrile (PAN) and poly(vinylpyrrolidone) (PVP) was dissolved in *N,N*-dimethylformamide (DMF). For electrospinning, a high voltage and feeding rate of ~13 kV and 0.03 ml h⁻¹, respectively, were employed. The distance between the syringe needle and the collector was fixed at ~15 cm. The as-spun nanofibres were stabilized at 280 °C for 5 h in air and then carbonized at 800 °C for 3 h in N₂ gas. The CNFs were subjected to acid treatment using a mixture (1:1 (v/v)) of HF and HNO₃, for the formation of –COOH, –OH, and >C=O functional groups on their surface. Then, the acid-treated CNFs were freeze-dried using liquid N₂ at –50 °C in order to ensure high porosity [11]. In order to obtain high loading of Pt electrocatalysts on the CNF–Ru core–shell supports, we carried out not room temperature drying but freeze-drying for synthesizing improved

* Corresponding author.

E-mail address: hjahn@seoultech.ac.kr (H.-J. Ahn).

mesoporous CNF supports. That is, the solvent in the samples after acid treatment of CNFs was completely vaporized by means of freeze-drying to possess their developed and controllable mesoporosity [12]. Thus, the introduction of freeze-drying is possible to obtain improved mesoporosity of the CNF supports, resulting in high dispersion of Ru shell layers on the CNF supports. For fabrication of the CNF–Ru core–shell supports, the CNFs were dispersed in DI water with stirring and under ultrasonication and then 0 mM, 0.28 mM, 0.56 mM, and 0.84 mM $\text{RuCl}_3 \cdot x\text{H}_2\text{O}$ precursors were separately added to the corresponding samples of the abovementioned-CNF dispersion. Concentrated NaBH_4 solution (100 mg ml^{-1}) was used as a reducing agent for the formation of a metallic Ru shell layer on the CNFs, which were then dried at 80°C in an oven. The four types of supports were dipped in $0.56 \text{ mM H}_2\text{PtCl}_6 \cdot x\text{H}_2\text{O}$ solution and then added to a concentrated NaBH_4 solution to load 20 wt.% Pt. Thus, Pt-electrocatalyst-loaded CNF–0 wt.% Ru core–shell, CNF–10 wt.% Ru core–shell, CNF–20 wt.% Ru core–shell, and CNF–30 wt.% Ru core–shell supports were obtained (referred to as Pt/CNFs, A, B, and C), respectively. The resultant samples were washed several times with DI water and freeze-dried at -50°C . The morphological, structural properties, and chemical bonding states of these samples were observed by a field emission-scanning electron microscopy (FESEM; Hitachi

S-4800), transmission electron microscopy (TEM; JEOL 2100F, KBSI Suncheon center), X-ray diffractometry (XRD, Rigaku D/Max 2500V), and XPS (ESCALAB 250 equipped with an Al $K\alpha$ X-ray source). Electrochemical measurements on the samples were performed using a Potentiostat/Galvanostat (PGST302N by Eco Chemie) in a conventional three-electrode system, which consisted of a glassy carbon electrode (0.07 cm^2 , working electrode), Pt gauze (counter electrode), and a Ag/AgCl (sat. KCl, reference electrode). An electrolyte prepared using $0.5 \text{ M H}_2\text{SO}_4$ and $2 \text{ M CH}_3\text{OH}$ solutions were used. Electrochemical activities during methanol electrooxidation were characterized by performing cyclic voltammetry measurements in the range -0.2 to 1.0 V at a scan rate of 50 mV s^{-1} . Chronoamperometry was performed in a solution of $0.5 \text{ M H}_2\text{SO}_4$ and $2 \text{ M CH}_3\text{OH}$ at a constant potential of 0.5 V for 600 s.

3. Results and discussion

Fig. 1(a–e) shows FESEM images of the CNF supports, Pt/CNFs, sample A, sample B, and sample C. The diameters of the samples are in the range ~ 197 – 250 nm for the CNF supports, ~ 202 – 250 nm for Pt/CNFs, ~ 196 – 243 nm for sample A, ~ 198 – 250 nm for sample B, and ~ 209 – 257 nm for sample C. In addition, the plain

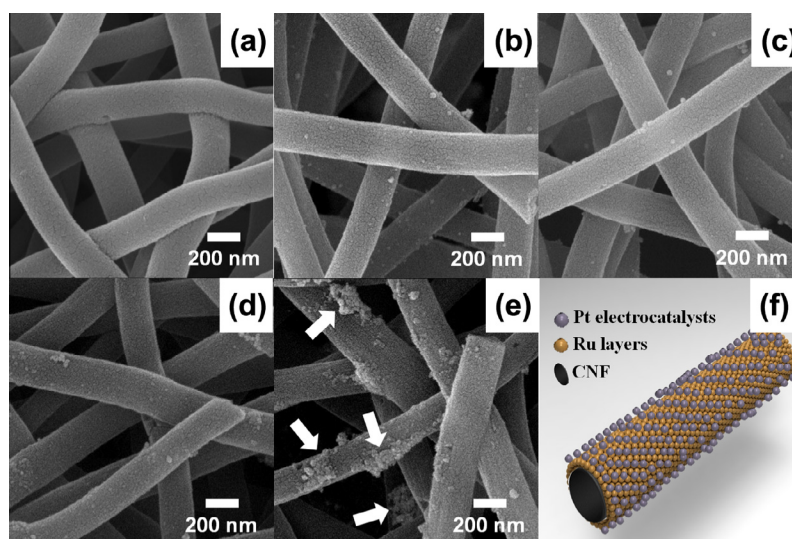


Fig. 1. SEM images of (a) CNF supports, (b) Pt/CNFs, (c) sample A, (d) sample B, and (e) sample C via electrospinning and a reduction method. (f) A schematic illustration of the Pt electrocatalyst-loaded CNF–Ru core–shell supports.

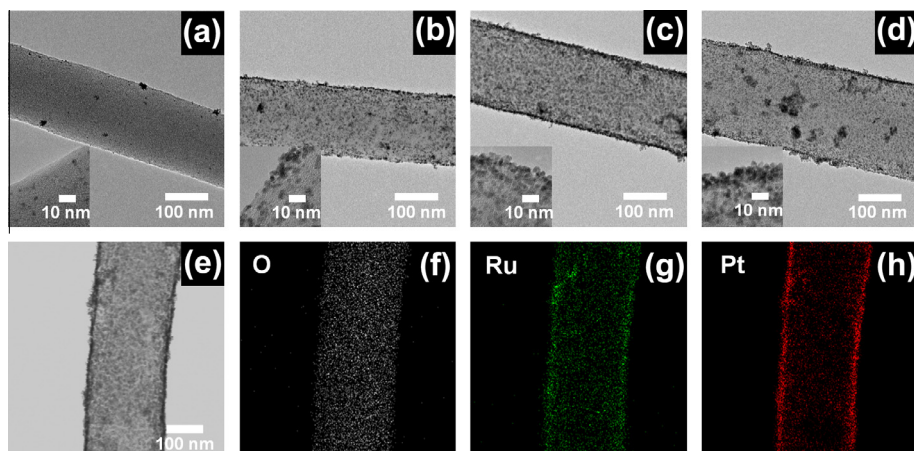


Fig. 2. (a–d) TEM images of Pt/CNFs, sample A, sample B, and sample C. (e–h) TEM–EDS mapping data obtained from sample B.

CNF supports have a smooth NF surface (Fig. 1(a)) but small Pt blobs are seen on the CNFs or CNF–Ru supports (Figs. 1(b–d)), implying that the Pt electrocatalyst is successfully loaded on the CNFs or CNF–Ru supports. Furthermore, sample C (Fig. 1(e)) exhibits a highly agglomerated surface because of the high loading (30 wt.%) of the Ru shell layer on the CNFs, which obstructed uniform dispersion of the Pt electrocatalysts. This agglomerated surface could result in reduced electrocatalytic activity for electrooxidation in DMFCs. Fig. 1(f) shows the schematic illustration of the ideal Pt-loaded CNF–Ru core–shell supports. Our strategy in this study was to optimize the loading of the Ru shell layer, because Pt electrocatalysts was not effectively loaded on a plain CNF surface.

Fig. 2(a–d) shows TEM images of Pt/CNFs, samples A, B, and C respectively. The Pt electrocatalyst, showing up as relatively dark

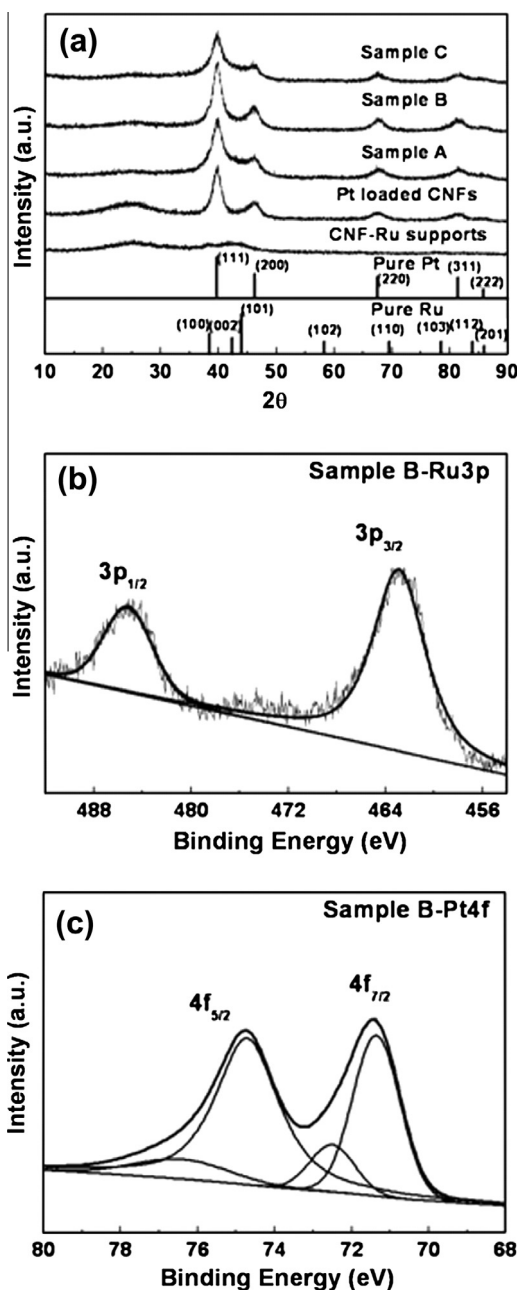


Fig. 3. (a) XRD data of CNF–Ru supports, Pt/CNFs, sample A, sample B, and sample C. XPS spectra of the (b) Ru 3p and (c) Pt 4f obtained from sample B.

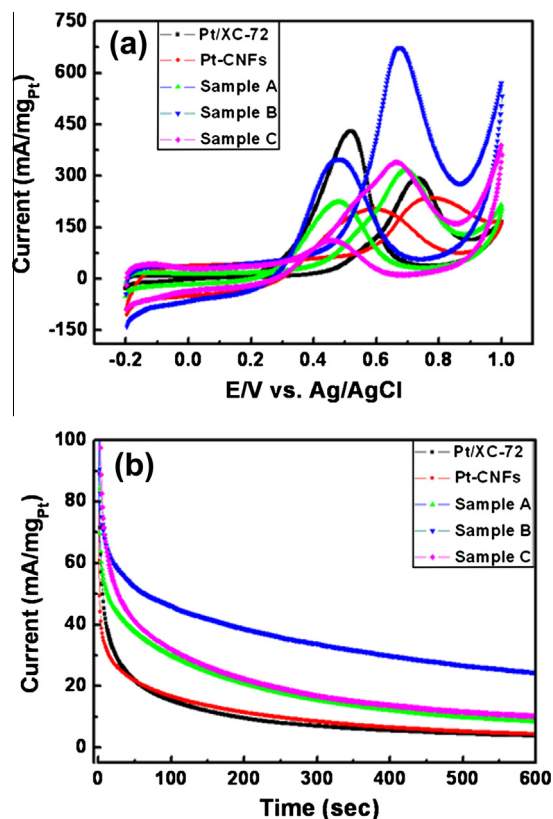


Fig. 4. (a) Cyclic voltammograms for methanol electrooxidation of Pt/CNFs, sample A, sample B, sample C, and commercial Pt/XC-72. (b) Chronoamperometry of Pt/CNFs, sample A, sample B, sample C, and commercial Pt/XC-72 characterized in a solution of 0.5 M H_2SO_4 and 2 M CH_3OH at 0.5 V.

blobs ($\sim 1\text{--}3$ nm), was sparsely distributed on the CNFs, which had a relatively bright-grey contrast (Fig. 2(a)). Thus, to overcome this problem, we employed the CNF–Ru core–shell supports with Pt electrocatalysts. Samples A, B, and C (Fig. 2(b–d)) showed the Pt electrocatalysts-loaded CNF–Ru core–shell supports. In particular, sample B exhibited the best dispersion of Pt on the CNF–Ru core–shell support because of optimum loading of the Ru shell layer. As shown in the insets of Fig. 2(b–d), sample B displayed excellent dispersion of electrocatalysts on the supports. Furthermore, sample C (Fig. 2(d)) showed relatively larger agglomerates of Pt because of the Ru shell layer loading. Fig. 2(e–h) presents TEM–EDS mapping data obtained from sample B to confirm the distribution and composition of Ru and Pt atoms on the CNFs. The EDS results indicate that Ru and Pt atoms are uniformly dispersed on the CNFs. In addition, the distribution of Pt atoms is slightly larger than that of Ru atoms, implying that the presence of the Pt electrocatalyst on the shell layer of the CNF–Ru core–shell supports.

Fig. 3(a) shows XRD data elucidating the structures and crystallinities of CNF–Ru supports, Pt/CNFs, sample A, sample B, and sample C. The main diffraction peaks of Pt/CNFs, sample A, sample B, and sample C are observed at $\sim 39.7^\circ$, 46.2° , 67.3° , and 81.3° , corresponding to the (111), (200), (220), and (311) planes of face-centred cubic Pt phases of the space group $Fm\bar{3}m[225]$ (JCPDS card No. 04-0802), respectively. Further, weak diffraction peaks due to the CNF–Ru supports are observed at $\sim 38.4^\circ$, 42.1° , and 44.0° , corresponding to the (100), (002), and (101) planes of Ru phases (hexagonal structure) of the space group $P6_3/mmc[194]$ (JCPDS card No. 06-0663). Broad diffraction peaks are observed at around 25.0° , indicating the amorphous nature of the CNF supports. In addition, diffraction peaks due to samples A, B,

and C do not appear to shift to higher angles, implying the absence of PtRu alloy but the presence of singular Pt and Ru phases. We carried out XPS measurements to investigate the chemical bonding states of the samples. Fig. 3(b and c) shows the XPS spectra of Ru 3*p* and Pt 4*f* core levels obtained from sample B. The XPS Ru 3*p* core levels of Ru 3*p*_{3/2} and Ru 3*p*_{1/2} photoelectrons are observed at ~462.6 eV and ~485.0 eV, corresponding to the metallic Ru phases [13]. Furthermore, the XPS Pt 4*f* core levels of Pt 4*f*_{7/2} and Pt 4*f*_{5/2} photoelectrons are observed at ~71.3 eV and ~74.4 eV. This implies that Pt phases are present as the zero-valent metallic states. The FESEM, TEM, XRD, and XPS results indicate the formation of Pt electrocatalyst-loaded the CNF–Ru core–shell supports.

Fig. 4(a) shows cyclic voltammograms of methanol electrooxidation of the samples. The higher the electrooxidation rate of methanol, the greater is the number of electrons produced at the anode ($\text{CH}_3\text{OH} + \text{H}_2\text{O} \rightarrow 6\text{e}^- + 6\text{H}^+ + \text{CO}_2$) [14]. Thus, the performance of DMFCs improved. The oxidation current densities for Pt/CNFs, sample A, sample B, and sample C are ~235.7, ~316.2, ~674.3, and ~339.7 mA mg_{Pt}⁻¹, respectively. The current density of Pt/XC-72 is ~292.6 mA mg_{Pt}⁻¹, which is in good agreement with previously reported results [15]. The electrocatalytic activity for methanol electrooxidation is directly associated with the current density. Therefore, sample B exhibits the best electrocatalytic activity among all the samples. In particular, the electrocatalytic activity of sample B is approximately 2.3 higher than that of commercial Pt/XC-72. This enhancement can be attributed to the excellent dispersion of the Pt electrocatalyst owing to the optimum loading of the Ru shell layer on the CNFs. Furthermore, the metallic Ru shell layer was well grown on the CNFs due to the same crystal structure with a hexagonal structure. Therefore, the optimum CNF–Ru core–shell supports improves the dispersion of Pt electrocatalysts and hence results in the large enhancement of methanol electrooxidation in DMFCs. However, sample C exhibits lower electrocatalytic activity because of the agglomerated Ru shell layer, as shown in the SEM image (see arrow) of Fig. 1(e). Furthermore, it is very difficult to load the Pt electrocatalyst on the plain CNF surface [16].

To investigate the electrocatalytic stability of the samples, chronoamperometry was performed (Fig. 4(b)). All samples exhibited a current decay during the initial stage because of the formation of interfering species such as CH₃OH_{ads} and CHO_{ads} and a subsequent current decay during methanol electrooxidation. Furthermore, a subsequent current decay of all catalysts can be attributed to the adsorbed SO₄²⁻ anions on the catalyst surface, which obstructs the methanol electrooxidation [17]. In spite of the hindrance of the adsorbed SO₄²⁻ anions, sample B exhibited a much slower current decay compared to the other samples up to 600 s. In other words, sample B showed superior electrocatalytic stability during the whole test range. That is, optimum loading (sample B) of the Ru shell layer on CNFs can provide highly uniform dispersion of the Pt electro-catalysts, which is less susceptible to the poisoning

of the catalysts due to the fixation of interfering species as previously reported [18]. Thus, these results imply that the use of optimum CNF–Ru core–shell supports can significantly improve catalytic activity and electrocatalytic stability, and thereby help in improving the performance of DMFCs.

4. Conclusion

Pt electrocatalysts-loaded CNF–Ru core–shell supports were synthesized via electrospinning and a reduction method. To examine the optimum loading conditions, four types of supports that differed in the Ru shell layer loading were synthesized. Among these supports, sample B exhibited superior electrocatalytic activity (~674.3 mA mg_{Pt}⁻¹) and superior electrocatalytic stability. The cause of the improved efficiency was the excellent dispersion of the Pt electrocatalysts, which in turn was due to the optimum Ru shell layer loading on the CNFs.

Acknowledgements

This research was supported by Basic Science Research Program through the National Research Foundation of Korea (NRF) funded by the Ministry of Education, Science and Technology (2012-007444).

References

- [1] S. Wasmus, A. Küver, *J. Electroanal. Chem.* 461 (1999) 14–31.
- [2] H.N. Dinh, X. Ren, F.H. Garzon, P. Zelenay, S. Gottesfeld, *J. Electroanal. Chem.* 491 (2000) 222–233.
- [3] A.S. Arico, V. Baglio, E. Modica, A. Di Blasi, V. Antonucci, *Electrochem. Commun.* 6 (2004) 164–169.
- [4] S. Sharma, B.G. Pollet, *J. Power Sources* 208 (2012) 96–119.
- [5] G.-H. An, H.-J. Ahn, *ECS Solid State Lett.* 2 (2013) M33–M36.
- [6] Y. Zhai, Y. Dou, D. Zhao, P.F. Fulvio, R.T. Mayes, S. Dai, *Adv. Mater.* 23 (2011) 4828–4850.
- [7] G.-H. An, H.-J. Ahn, *Ceram. Int.* 38 (2012) 3197–3201.
- [8] Q. Zhou, P. Li, X. Wang, X. Zhou, D. Yang, D. Chen, *Mater. Chem. Phys.* 126 (2011) 41–45.
- [9] D. Sebastián, A.G. Ruíz, I. Suelves, R. Moliner, M.J. Lázaro, V. Baglio, A. Stassi, A.S. Arico, *Appl. Catal. B* 115 (2012) 269–275.
- [10] S. Kang, S. Lim, D.-H. Peck, S.-K. Kim, D.-H. Jung, S.-H. Hong, H.-G. Jung, Y. Shul, *Int. J. Hydrogen Energy* 37 (2012) 4685–4693.
- [11] S.L. Candelaria, R. Chen, Y.-H. Jeong, G. Cao, *Energy Environ. Sci.* 5 (2012) 5619–5637.
- [12] T. Yamamoto, T. Ohmori, Y.H. Kim, *Micropor. Mesopor. Mater.* 112 (2008) 211–218.
- [13] C. Bock, C. Paquet, M. Couillard, G.A. Botton, B.T. Macdougall, *J. Am. Chem. Soc.* 126 (2004) 8028–8037.
- [14] J. Prabhuram, T.S. Zhao, H. Yang, *J. Electroanal. Chem.* 578 (2005) 105–112.
- [15] F. Su, Z. Tian, C.K. Poh, Z. Wang, S.H. Lim, Z. Liu, J. Lin, *Chem. Mater.* 22 (2010) 832–839.
- [16] S.L. Knupp, W. Li, O. Paschos, T.M. Murray, J. Snyder, P. Haldar, *Carbon* 46 (2008) 1276–1284.
- [17] Z. Ji, X. Shen, G. Zhu, K. Chen, G. Fu, L. Tong, *J. Electroanal. Chem.* 682 (2012) 95–100.
- [18] H. Gharibi, M. Amani, H. Pahlavanzadeh, M. Kazemini, *Electrochim. Acta* 97 (2013) 216–225.